This document is the accepted manuscript version of the following article:
Berens, M. J., Hofstetter, T. B., Bolotin, J., & Arnold, W. A. (2020). Assessment of 2,4-dinitroanisole transformation using compound-specific isotope analysis after in situ chemical reduction of iron oxides. Environmental Science and Technology, 54(9), 5520-5531. https://doi.org/10.1021/acs.est.9b07616

Assessment of 2,4-dinitroanisole transformation using compound-specific isotope analysis after in situ chemical reduction of iron oxides

Matthew J. Berens[†], *Thomas B. Hofstetter*[‡], *Jakov Bolotin*[‡], *and William A. Arnold**[,†]

[†]Department of Civil, Environmental, and Geo- Engineering, University of Minnesota, 500 Pillsbury Drive SE, Minneapolis, MN, 55455-0116, United States

[‡]Eawag, Swiss Federal Institute of Aquatic Science and Technology, Department of Environmental Chemistry, Überlandstrasse 133, CH-8600 Dübendorf and Institute of Biogeochemistry and Pollutant Dynamics, ETH Zürich, CH-8092 Zürich, Switzerland

*Corresponding author: William A. Arnold; Phone: 612-625-8582; e-mail: arnol032@umn.edu

ABSTRACT

Ferrous iron-bearing minerals are important reductants in the contaminated subsurface but their availability for the reduction of anthropogenic pollutants is often limited by competition with other electron acceptors including microorganisms and poor accessibility to Fe(II) in complex

hydrogeologic settings. The supply of external electron donors through *in situ* chemical reduction (ISCR) has been proposed as one remediation approach but the quantification of pollutant transformation is complicated by the perturbations introduced to the subsurface by ISCR. Here, we evaluate the application of compound specific isotope analysis (CSIA) for monitoring the reduction of 2,4-dinitroanisole (DNAN), a component of insensitive munitions formulations, by mineral-bound Fe(II) generated through ISCR of subsurface material from two field sites. Electron balances from laboratory experiments in batch and column reactors showed that 3.6% to 11% of the total Fe in the sediments was available for the reduction of DNAN and its partially reduced intermediates after dithionite treatment. The extent of DNAN reduction was successfully quantified from its N isotope fractionation measured in the column effluent based on the derivation of a N isotope enrichment factor, ε_N, derived from a comprehensive series of isotope fractionation experiments with numerous Fe(II)-bearing minerals as well as dithionite-reduced subsurface materials. Our observations illustrate the utility of CSIA as a robust approach to evaluate the success of *in situ* remediation through abiotic contaminant reduction.

INTRODUCTION

Ferrous iron (Fe(II)) associated with Fe-bearing minerals (e.g., iron (oxyhydr)oxides, clays, sulfide minerals) is an important reductant of many subsurface pollutants.[1–6] Despite an abundance of Fe(II) in the anoxic subsurface, pollutant reduction is often limited through competition with other potential electron acceptors and restricted pollutant transport and accessibility to reactive Fe(II)-bearing minerals in response to local hydrogeologic conditions. Several approaches have been evaluated to enhance the availability of reactive Fe(II) including biostimulation,[7,8] bioaugmentation,[9,10] additions of external electron donors (i.e., *in situ* chemical reduction; ISCR)

including dithionite, [11,12] polysulfides,[13] and (sulfidized) ZVI,[14,15] and combinations thereof.[16] To date, several of these strategies have been successfully applied to a number of environmental contaminants including heavy metals[12,17,18] and chlorinated solvents.[14,19,20]

One major challenge when applying an *in situ* (bio)remediation technique is providing a reliable evaluation of performance; it is difficult to quantify the amount of transformed contaminants from concentration measurements alone.[21–23] For example, the need to (repeatedly) inject aqueous solutions containing electron donors into the subsurface introduces perturbations that may lead to pollutant dilution without degradation. Moreover, reduction of Fe(III) induces partial reductive dissolution and transformation of reactive Fe minerals and could mobilize solid-bound contaminants.[17,24–26]

Compound specific isotope analysis (CSIA) is used to evaluate the extent of contaminant remediation by quantifying isotope enrichment of one or more elements in the residual pollutant.[27–32] Because changes in stable isotope ratios (e.g., $^{15}N/^{14}N$, $^{13}C/^{12}C$) reflect reactions in which bond-cleavage occurs, isotope fractionation is minimally affected by non-degradative processes (e.g., sorption, dilution, phase transfer), thus circumventing many of the challenges associated with monitoring pollutant removal by concentration measurements alone.[33,34] Despite the incorporation of CSIA into published monitored natural attenuation protocols, the majority of efforts have focused on biodegradation.[21,27,28,35–37]

The recent emergence of 2,4-dinitroanisole (DNAN) in insensitive munitions formulations has caused concern because of its potential to contaminate large areas of land and water.[38,39] We previously provided the first assessment of C and N isotope fractionation during abiotic DNAN reduction[40] but did not consider reductants beyond synthetic Fe-minerals. The Fe(II)-mediated reduction of DNAN generated isotope fractionation patterns that were indicative of certain reaction

pathways yet independent of DNAN reaction rates and solution chemistry (e.g., organic matter).[40] Given the heterogeneity of natural soils and sediments and the crystallographic diversity of Fe-minerals, however, it remains to be understood if DNAN isotope fractionation during reduction by Fe(II) of natural minerals deviates from that observed with synthetic analogs. Because multiple amendments of a given reductant are often required to achieve remediation targets with ISCR,[12,41,42] it is similarly unknown how multiple redox cycles will affect the interpretation of CSIA results. Our findings suggest that because DNAN reduction by mineral-associated Fe(II) follows a common reaction pathway (i.e., abiotic nitro-group reduction[28,35,40,43–45]), the associated isotope fractionation will not be affected despite the use of synthetic minerals or naturally collected ferruginous soils and sediments. This understanding could allow for DNAN to be a surrogate for other nitroaromatic compounds (NACs) including 2,4,6-trinitrotoluene (TNT) and analogs of nitrobenzene in the subsurface[46] and is important given the continuing need for *in situ* remediation techniques.[47] Numerous studies have indeed reported similar isotope enrichment factors from the abiotic reduction of several NACs in a range of experimental laboratory systems.[43–45]

In this study, we explored the application of CSIA for monitoring DNAN reduction during dithionite-based ISCR schemes. Sodium dithionite ($Na_2S_2O_4$) was chosen as the reductant because of its previous success for pollutant remediation in contaminated aquifers.[11,19,41,48] We tested the reactivity of several Fe-bearing minerals and Fe-mineral containing sediments to promote DNAN reduction in batch reactors receiving amendments of aqueous Fe(II) and those receiving ISCR and used the distributions of reaction products to track the number of reduction equivalents transferred. The N and C isotope fractionation was measured during batch experiments to determine the bulk isotope enrichment factors (ε_N and ε_C) and apparent kinetic isotope effects (^{15}N-AKIE and ^{13}C-AKIE) associated with DNAN reduction. To simulate reducing environmental conditions,

subsurface materials collected from two field sites were exposed to DNAN following ISCR in continuous-flow column reactors. A modified Rayleigh equation was used to make quantitative estimates of DNAN degradation from N isotope ratios ($\delta^{15}N$) measured during each experiment. The accuracy of this approach was evaluated by conducting statistical comparisons of predicted versus observed extent of DNAN degradation.

MATERIALS AND METHODS

A complete list of chemicals used in this study is provided in the Supporting Information (SI).

Laboratory conditions. All syntheses and batch experiments were performed in an anaerobic chamber (Coy Laboratory Products Inc.) with a 95% N_2/5% H_2 atmosphere. Column experiments were performed in a NexGen anaerobic glovebox (Vacuum Atmospheres Company) maintained at <1 ppm O_2 with N_2 balance. Ultrapure water (≥18.2 MΩ•cm) was generated by a Milli-Q Academic system (MilliporeSigma) and used to prepare all aqueous solutions. The ultrapure water was purged with N_2 gas (99.99%, Matheson) for at least 2 h prior to transfer into the chamber. Methanolic stock solutions were similarly prepared in deoxygenated methanol (ACS grade, MilliporeSigma). Laboratory equipment and reagents were evacuated in the exchange chamber and equilibrated overnight in the glovebag before use.

Material preparation and characterization. Subsurface materials were collected from the Twin Cities Army Ammunition Plant (TCAAP; Arden Hills, MN) and the Tinker Air Force Base (Tinker AFB; Oklahoma City, OK). Both sites have a history of contamination by organic pollutants and have required remediation efforts.[1,49] Aquifer material from TCAAP was collected from the saturated zone by sonic drilling to a depth of 41–45 m. The material was dried, purged with N_2 gas, and stored inside the anaerobic chamber. Shallow sediment collected from Tinker

AFB was dried at 100 °C and stored in an amber jar under laboratory atmosphere. Both TCAAP and Tinker AFB materials were sieved by particle size to 350–425 μm before use. Synthetic magnetite nanoparticles were obtained from our previous work[40] and a suspension of rhombohedral hematite in deoxygenated, ultrapure water (~15 g/mL) was acquired from Voelz et al.[50]

Each material was characterized by X-ray diffraction (XRD; Figure S1) to evaluate the purity (synthetic minerals) and bulk mineralogy (natural materials). No additional peaks were detected in patterns collected from synthetic minerals. The primary Fe-bearing phase as detectable by XRD in natural materials was magnetite (Fe_3O_4; TCAAP)[1,51] and hematite (Fe_2O_3; Tinker AFB). Quartz (SiO_2; PDF #46-1045) was detected in each collected material as expected for highly weathered systems.

The total iron content (Fe_T) of TCAAP and Tinker AFB materials was quantified by inductively coupled plasma optical emission spectroscopy (ICP-OES). The ratio of Fe(II)/Fe(III) was estimated by acid dissolution in 3 M HCl[52,53] and quantification by the ferrozine method[54] (Section S3). The amount of ion-exchangeable Fe(II) was estimated by saturating each material in 1 M $CaCl_2$ for 7 d and was below the limit of quantification in all samples (data not shown).[55] The magnetic portion of the TCAAP sediment (hereafter termed "TCAAP extract") was separated from the bulk material with a neodymium magnet as described by Strehlau et al.[51] and characterized by the same analyses. A summary of the relevant chemical and physical properties of all materials is provided in Table S1. Additional characterizations of hematite[50] and magnetite[51] are reported elsewhere.

***In situ* chemical reduction.** For batch experiments receiving ISCR treatment, Fe-bearing materials were suspended in a solution of $K_2CO_3/S_2O_4^{2-}$ (2:1 mol/mol) and rotated for 24 h, at

which point the suspension was separated via centrifugation and the supernatant discarded. The dithionite concentrations were selected so that enough dithionite was added to theoretically reduce one-tenth of the total Fe present (i.e., 1 mol $S_2O_4^{2-}$:20 mol Fe_T; see eq 1). The $K_2CO_3/S_2O_4^{2-}$ ratio was chosen to buffer the 4 moles of H^+ released per 1 mole of dithionite consumed during iron reduction (eq 1).

$$S_2O_4^{2-} + 2Fe^{3+} + 2H_2O \rightarrow 2Fe^{2+} + 2SO_3^{2-} + 4H^+ \quad (1)$$

The treated materials were then washed three times with carbonate buffer (10 mM, pH 7) by centrifugation to remove excess dithionite and its reaction products (e.g., sulfate, sulfite, thiosulfate),[11] suspended in carbonate buffer, and immediately used for DNAN reduction experiments in batch reactors. The Fe(II) content of each reduced material after ISCR was determined by acid dissolution as described above.

For column experiments, the materials were conditioned before adding dithionite by passing carbonate buffer (10 mM, pH 7.0) upwards through the column at 0.5 mL/min for 5 pore volumes. An aqueous solution of 1.25 mM sodium dithionite and 2.50 mM K_2CO_3 (pH 8–9) was then fed upward to the column at 0.25 mL/min for ~18–20 h. The low flow rate and long run (~30 pore volumes) time were used to allow enough time for the reaction to occur. Columns were flushed with ~10 pore volumes of carbonate buffer to remove unreacted dithionite and any oxidized sulfur species. The exact amounts of pore volumes were chosen so that the same total amount of dithionite:Fe was introduced to each system (see eq 1). The total amount of iron in each column was in 20-fold excess to the dithionite added (i.e., 1 mol $S_2O_4^{2-}$:20 mol Fe_T) to target a reduction of one-tenth of Fe_T. Anoxic dithionite-buffer solutions were prepared fresh before each experiment to avoid loss of dithionite by aqueous disproportion; the rate of dithionite loss by aqueous disproportionation, however, has shown to be slower than Fe(III) reduction by dithionite.[19]

Batch experiments. Batch reactors were prepared in 35 mL borosilicate serum bottles according to previously described procedures.[40] First, a suspension of an untreated or dithionite-reduced Fe-bearing mineral in 10 mM carbonate buffer (pH 7.0) was added to each reactor. Solid loadings were varied from 1.0 g/L (hematite) to 143 g/L (TCAAP) such that DNAN transformation occurred in a similar time period. Aqueous Fe(II) was added to a concentration of 1 mM in reactors containing untreated materials. The dithionite-reduced materials did not receive amendments of Fe(II). Reactors were equilibrated for 21–24 h on an end-over-end rotator (Glas-col) at 40 rpm at which point the pH and aqueous Fe(II) concentration (via the Ferrozine assay;[54] Section S3) were measured. If necessary, the pH was adjusted back to 7.0 with 1 M HCl or 1 M NaOH and the aqueous Fe(II) content was restored to 1 mM in the reactors to which Fe(II) was added. Reactions were initiated by spiking DNAN from a methanolic stock solution to an initial concentration of 200 μM. Reactors were placed on the rotator (40 rpm) and sacrificed at appropriate time points for concentration and stable isotope analyses. The pH (all reactors) and Fe(II) concentrations (Fe(II) amended reactors only) were closely monitored during reactions and maintained at 7.0 and 1 mM, respectively. Reactions were quenched by filtration through a 0.2 μm nylon syringe filter (Chrom Tech) and stabilized with 1 M HCl (trace metals grade, MilliporeSigma) to pH<4 to prevent iron precipitation; DNAN did not react with aqueous Fe(II) under these conditions (data not shown). A portion (~1 mL) of each sample was analyzed for DNAN and intermediate/product concentrations by high pressure liquid chromatography (HPLC; method in SI) and the remaining sample (~18 mL) was stored at 4 °C for CSIA of DNAN.

The quantity of reduction equivalents transferred to DNAN from each reduced material was calculated with the assumption that 6 moles of electrons are required to reduce one nitro-moiety to the corresponding amine (see Scheme S1). The reduced products typically generated during

abiotic DNAN reduction are 2-amino-4-nitroanisole (2-ANAN), 4-amino-2-nitroanisole (4-ANAN), and 2,4-diaminoanisole (DAAN). Thus, 6 and 12 electrons are required for each mole of 2/4-ANAN and DAAN formed during DNAN reduction, respectively (Section S4 and eq S1).

Reactions in sediment columns. Borosilicate glass columns (Kimble FLEX-COLUMNS®; 2.5 cm I.D., 10 cm length) were packed with each natural material to uniform bulk (ρ_b = 1.66 ± 0.04 g/cm^3) and particle densities (ρ_p = 2.68 ± 0.05 g/cm^3). The mean porosity of sediment columns was 0.44 ± 0.05 (see Table S2). A flow adapter (Kimble) with fluorinated ethylene propylene (FEP) tubing was secured to the column inlet to prevent sediment migration and facilitate accurate bed height calculations. A polypropylene end cap was fixed at the column outlet. All feed solutions were amended with 10 mM NaCl to prevent the precipitation of insoluble species which may cause changes to flow characteristics. Pore volume and porosity were determined by saturating with 10 mM NaCl and a step input conservative tracer (100 mM NaBr) was used to characterize column flow and estimate the dispersion coefficient (Table S2; fitting details in SI). Bromide concentrations at the column outlet were measured with a conductivity probe (Oakton). Dispersion coefficients prior to experiments were 2.38 ± 0.24 and 2.53 ± 0.12 cm^2 s^{-1} for TCAAP and Tinker AFB columns, respectively, at a flow rate of 0.5 mL/min. All column materials were then reduced by sodium dithionite before experiments using DNAN.

Columns were equilibrated prior to DNAN reduction experiments by upward flow (0.5 mL/min) with 10 mM, pH 7.0 carbonate buffer including 10 mM NaCl for 5 pore volumes. Reactions were initiated by adding DNAN (200 μM) to the feed solution and collecting effluent samples with an automated fraction collector (Bio-Rad Laboratories Inc). Experiments were terminated once the effluent concentration was equal to that of the feed solution. Columns were then flushed with carbonate buffer for several pore volumes to remove residual DNAN and any reaction products.

The column materials were then reduced again by sodium dithionite according to the method described above before further experiments using DNAN. The total number of reduction equivalents transferred to DNAN were calculated by integrating the concentrations of 2/4-ANAN and DAAN measured in the effluent (eq S2).

Compound specific isotope analysis. $^{13}C/^{12}C$ and $^{15}N/^{14}N$ isotope ratios of DNAN were measured following previously established procedures for gas chromatography / isotope ratio mass spectrometry (GC/IRMS) and solid phase micro extraction (SPME arrow) and are detailed in the Supporting Information.[40,56–59] Isotope signatures were calculated from isotope ratios according to eq S4 relative to Vienna PeeDee Belemnite ($\delta^{13}C_{VPDB}$) and air ($\delta^{15}N_{air}$) reference standards.[60] Carbon and nitrogen isotope enrichment factors (ε_C, ε_N) were calculated by non-linear regression of C and N isotope signatures ($\delta^{13}C$, $\delta^{15}N$) vs the fraction of remaining substrate (c/c_0) as shown in eq 2.[59]

$$\frac{\delta^{h}E+1}{\delta^{h}E_0+1} = \left(\frac{c}{c_0}\right)^{\varepsilon_E} \quad (2)$$

where $\delta^{h}E_0$ is the initial isotope ratios of DNAN ($\delta^{13}C_0$ = -37.4 ± 0.1‰, $\delta^{15}N_0$ = -2.4 ± 0.1‰) as evaluated by elemental analysis (EA)/IRMS. Apparent kinetic isotope effects (^{13}C-AKIE, ^{15}N-AKIE) were determined from eq 3 based on the methods outlined by Elsner et al.[61]

$$^{h}E\text{-AKIE} = \frac{1}{1+n*\varepsilon_E} \quad (3)$$

where n is a correction for isotopic dilution (n = 2 for primary ^{15}N-AKIEs and n = 1 for secondary ^{13}C-AKIEs). A linear regression of N and C isotope signatures was used to evaluate two-dimensional isotope fractionation trends. The slope of this regression ($\Lambda^{N/C}$) was calculated using both a simple linear regression model and the York method described by Ojeda et al.[62] and is approximately equal to the ratio of the bulk isotope enrichment factors ($\varepsilon_N/\varepsilon_C$). Because values of

223 $\Lambda^{N/C}$ from our previous work[40] were calculated by simple linear regression, in this report the result
224 of the York method is provided as an additional reference.

225 To estimate the extent of DNAN transformation (*F*) during column experiments, measurements
226 of $\delta^{15}N$ at the breakthrough front were applied to a modified form of the Rayleigh fractionation
227 equation (eq 4)[27] using an ε_N that was calculated based on the results of multiple datasets. This
228 combined ε_N value (ε_N^*) was obtained by plotting all $\delta^{15}N$ measurements (n = 122) from batch
229 experiments of DNAN reduction in this study and in Berens et al. [40] and performing a non-linear
230 regression of the combined data according to eq 2. The extent of DNAN reduction was calculated
231 with eq 4 from the deviation of measured $\delta^{15}N$ values from $\delta^{15}N_0$. using the combined ε_N^* value.
232 Note that eq 4 is the result of a reorganization of eq 2 to account for ε_N^*. We evaluated the accuracy
233 of our estimates by performing a linear regression of the predicted vs measured values of c/c_0 and
234 calculating the mean absolute error (MAE) of the predictions (eq 5).

235
$$F = \frac{c}{c_0} = \left(\frac{\delta^{15}N + 1}{\delta^{15}N_0 + 1}\right)^{1/\varepsilon_N^*} \quad (4)$$

236
$$\mathrm{MAE} = \frac{\sum_{i=1}^{n} \left| \left(c/c_{0,\,\mathrm{measured}}\right)_i - \left(c/c_{0,\,\mathrm{predicted}}\right)_i \right|}{n} \quad (5)$$

237

238 RESULTS AND DISCUSSION

239 **Kinetic studies in batch reactors.** Reduction of DNAN occurred in all reactors receiving
240 amendments of aqueous Fe(II) (Figure 1a, open symbols) or ISCR by sodium dithionite (Figure
241 1a, closed symbols). DNAN reduction was not observed in reactors containing only untreated
242 minerals or aqueous Fe(II) alone (Figure S2). This supports the current understanding that Fe(II)-
243 surface associations are required to mediate contaminant,[2,63–67] and in particular DNAN,[40]
244 reduction. The transformation products detected during DNAN reduction were 2-ANAN, 4-

ANAN, and DAAN (Figure 1b). X-ray diffraction (XRD) patterns collected before and after ISCR showed no detectable changes in mineral composition following the treatments (Figure S1) which suggests that the primary effect of ISCR on the structures of hematite and magnetite was the generation of surface-associated Fe(II) from oxide-Fe(III).

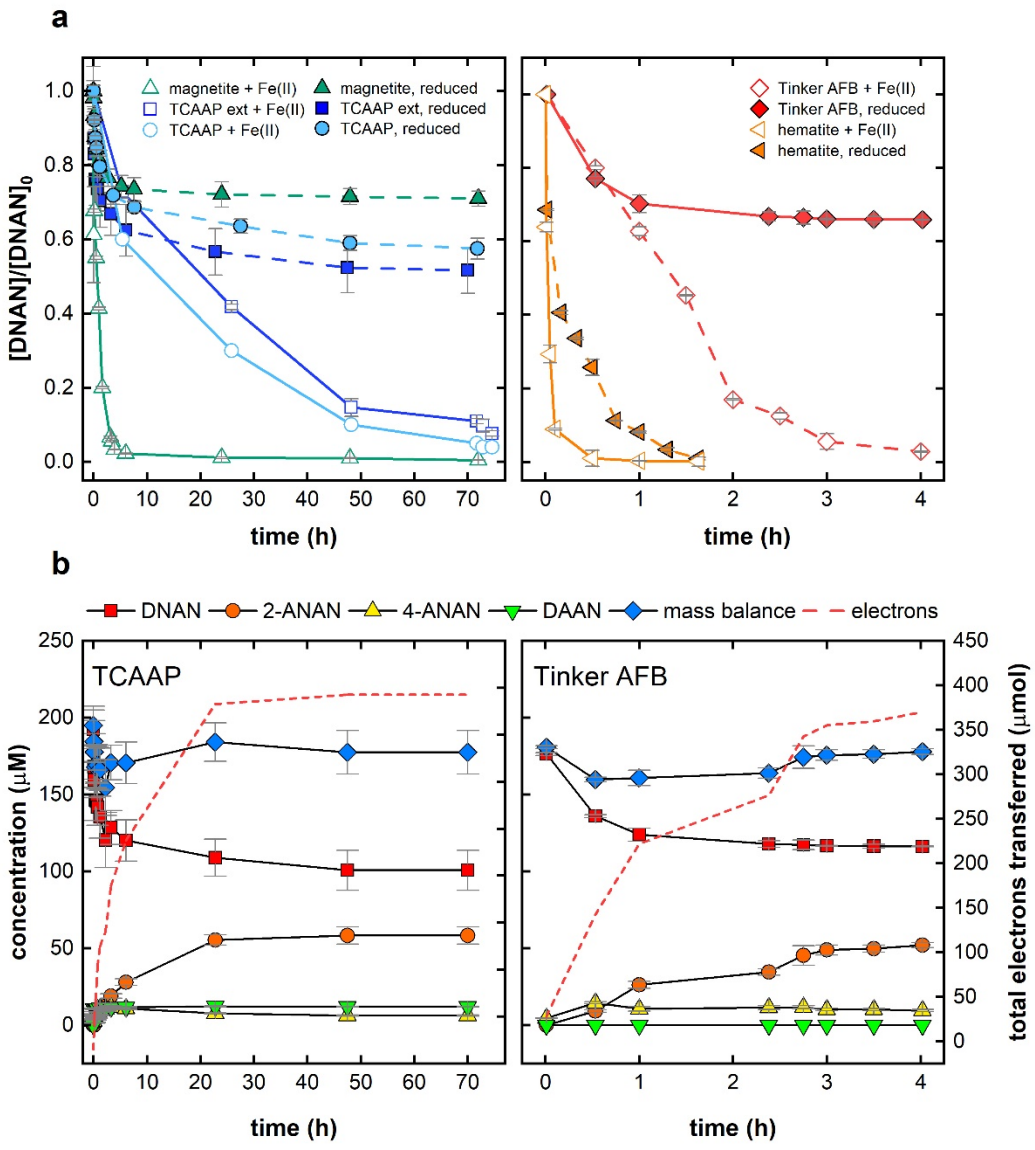

Figure 1. (a) Concentrations of DNAN during abiotic reduction by natural (TCAAP and Tinker AFB) and synthetic Fe-bearing (magnetite and hematite) materials. Experiments were performed with either untreated materials in the presence of 1 mM aqueous Fe(II) (open symbols) or with dithionite-reduced materials without additional Fe(II) (closed symbols). (b) Concentrations of DNAN, 2-ANAN, 4-ANAN, DAAN, and the cumulative number of electrons transferred during

DNAN reduction by reduced TCAAP (left) and Tinker AFB (right) materials. All error bars represent standard deviations of triplicate reactors. Note the difference in time scales.

When aqueous Fe(II) was maintained (1 mM) throughout the batch experiments, all of the added DNAN was reduced to 2/4-ANAN or subsequently DAAN by each of the untreated minerals (Figure 1a, open symbols). In reactors receiving ISCR, only a portion of the DNAN was removed (Figure 1a, closed symbols), likely because of a limited supply of available electron equivalents (i.e., mineral-associated Fe(II)) generated during ISCR. To understand the extent of DNAN reduction in systems receiving ISCR, an electron balance was computed for each set of reactions (Figure 1b, dashed line). Accounting for the number of electrons transferred to DNAN as a function of the mineral-associated Fe(II) (i.e., mol e^-/mol Fe(II)) allowed for an evaluation of the efficiency of ISCR to generate reactive Fe(II).

Dithionite-reduced magnetite, TCAAP extract, and hematite promoted DNAN reduction with extents of electron transfer ranging from 0.359–0.603 mol e^-/mol Fe(II) (Table 1). These results suggest that not all available iron (Fe_T) was reduced to reaction-accessible Fe(II)[68] during ISCR. The washing of materials following dithionite treatments may have caused the release of Fe(II) that was not retained on mineral surfaces. It is also possible that potentially reducible oxide-Fe(III) was inaccessible to dithionite.[69–72]

The lower standard reduction potential (E_H^0) of hematite/Fe(II) (+0.793 V) versus magnetite/Fe(II) (+1.053 V)[73] may further explain the difference in electron transfer between the two systems. The reactivity of Fe-bearing minerals for pollutant reduction increases with lower E_H values as evidenced by hematite experiments. Moreover, magnetite stoichiometry (x = Fe(II)/Fe(III)) directly correlates with its intrinsic E_H values[74] and reactivity towards NAC reduction.[75] The magnetite used in this study ranged from partially oxidized (x = 0.1, TCAAP

279 extract) to fully reduced, stoichiometric (x = 0.5, synthetic magnetite) materials. Low
280 stoichiometry magnetite is a better oxidant and was thus more easily reduced by dithionite than
281 the high stoichiometry magnetite (Table S1). These results emphasize the potential benefits of
282 ISCR to magnetite-bearing soils and sediments in which partially oxidized magnetite is common
283 and may be amenable to ISCR leading to more stoichiometric and thus reactive magnetite.[76,77]

284

285 **Table 1.** Total iron (Fe_T) and Fe(II) content of materials after dithionite treatments, and the
286 cumulative number electrons transferred during DNAN reduction experiments.

system	Fe_T (µmol)	Fe(II) (µmol)[c]	total e^- transferred (µmol)[d,e]	mol e^-/mol Fe(II)[e]
batch				
TCAAP	3430[a]	170	393 ± 1	2.31 ± 0.01
TCAAP extract	865[a]	432	232 ± 1	0.536 ± 0.003
magnetite	903[b]	451	162 ± 0.3	0.359 ± 0.001
Tinker AFB	2180[a]	79.1	370 ± 0.4	4.68 ± 0.01
hematite	439[b]	219	132 ± 1	0.603 ± 0.006
column				
TCAAP	25800[a]	1280	183 ± 30	0.143 ± 0.022
Tinker AFB	17000[a]	616	109 ± 10	0.176 ± 0.020

[a]Determined by ICP-OES. [b]Calculated from structural formulas of pure minerals. [c]Calculated by acid dissolution and quantification by the ferrozine method.[54] [d]Calculated using eqs S1–2. [e]Uncertainties represent standard deviations of triplicate reactors.

287

288 The number of reduction equivalents transferred to DNAN from dithionite-reduced TCAAP
289 (2.31 ± 0.01 mol e^-/mol Fe(II)) and Tinker AFB (4.68 ± 0.01 mol e^-/mol Fe(II)) materials exceeded
290 the initial amount of Fe(II) present after dithionite treatments (Table 1). Despite targeted dithionite
291 dosages to reduce one-tenth of the Fe_T, the calculated reduction efficiencies (i.e., Fe(II)/Fe_T from
292 data in Table 1) of TCAAP and Tinker AFB materials during ISCR were only 4.95% and 3.62%,
293 respectively. The low reduction efficiencies suggest that other reducible moieties were present in
294 the natural materials which were reduced by dithionite and subsequently provided reducing
295 equivalents for DNAN reduction.[78,79] For example, the reversible transfer of electrons in the

296 environment is often mediated by natural organic matter and humic substances, specifically those
297 containing quinone moeities[80–83], and the TCAAP and Tinker materials contained 0.46% (w/w)
298 and 0.88% (w/w) organic matter, respectively. The electron-carrying capacity of these species
299 plays a key role in both the reduction of substituted nitrobenzenes[84] and ferric iron.[85] Another
300 possibility is that acid digestion of the materials to determine Fe(II) was incomplete. This is
301 especially likely in materials with high Si content, such as phyllosilicates, because the Fe(III) is
302 easily reduced by dithionite but Fe(II) extraction requires a rigorous treatment with H_2SO_4 and
303 HF.[68,86,87] This fraction of Fe(II) is a known strong reductant of NACs.[3,88] The prominence of SiO_2
304 (Figure S1) and low Fe_T content of TCAAP and Tinker AFB materials (Table S1) suggests that a
305 large share of Fe_T was associated with silicates.

306 **Reactions in packed columns.** To probe for the availability of reduction equivalents in flow-
307 through systems, DNAN (200 μM) was introduced to column reactors containing dithionite-
308 reduced TCAAP or Tinker AFB materials for five cycles of Fe(III) reduction by dithionite
309 followed by DNAN exposure (Figure 2a-b). As shown in Figures 2c-d, ISCR in column reactors
310 generated reaction-accessible electron equivalents in natural materials and promoted the reductive
311 transformation of DNAN with a similar product distribution to the batch experiments (Figures 1c-
312 d, Figure S3). It should be noted that DAAN concentrations exceeded the input DNAN
313 concentration (up to 150%) during the early stages of experiments. To assess this phenomenon,
314 the cumulative amount of DAAN measured in the column effluent was compared to the total
315 amount of DNAN introduced. We found that the amount of DAAN in the peaks did not exceed the
316 total amount of DNAN introduced to the columns. This indicated that DAAN was either associated
317 with or retained on mineral surfaces and was then displaced by another solute, namely DNAN or

2/4-ANAN. The initial rapid production of DAAN leading to high concentration may have driven this interaction, and as aqueous concentrations dropped, other components in

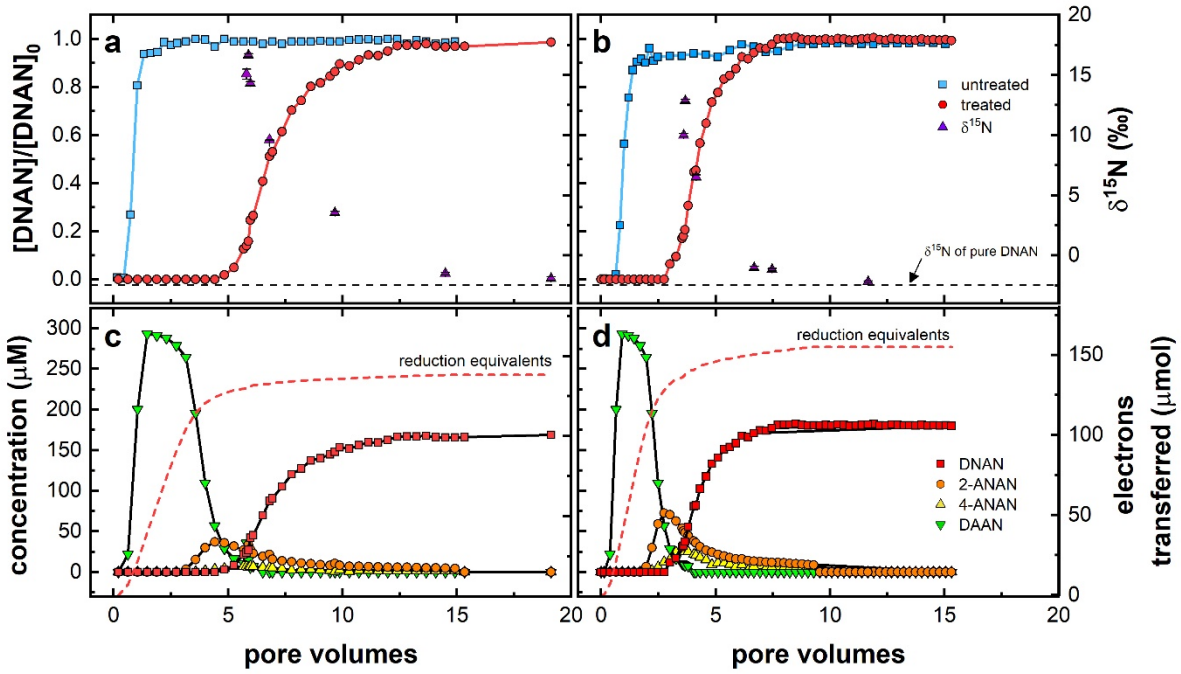

Figure 2. Breakthrough curves for 200 μM DNAN in (a) TCAAP and (b) Tinker AFB packed columns before (squares) and after (circles) receiving ISCR. Triangles denote measurements of $\delta^{15}N$ of DNAN in the effluent from treated columns. Error bars denote standard deviations from five sequential breakthrough experiments. Aqueous concentrations of DNAN (circles), 2-ANAN (squares), 4-ANAN (triangles), and DAAN (diamonds) during DNAN exposure to (c) TCAAP and (d) Tinker AFB columns. Dashed lines represent the cumulative number of reduction equivalents transferred to DNAN during experiments. The data provided in panels c and d are a representation of one of the reduction-reaction cycles shown in panels a and b, respectively. Individual cycles are shown in Figure S3.

the solution displaced DAAN from the surface. Such competition and effluent concentrations exceeding influents have been observed for ion sorption on activated carbon.[89] Another possible explanation is that a reaction intermediate (e.g., a hydroxylamine) is more strongly retained by the solid phase, as previously observed during the reduction of cyanonitrobenzene,[90] and the excess DAAN observed occurs once this intermediate has been reduced and released.

Despite ISCR targets that were equivalent to batch experiments (i.e., 10% reduction of Fe_T), the extent of electron transfer to DNAN from the reduced materials was markedly lower in columns than in batch experiments (0.143 ± 0.022 and 0.176 ± 0.020 mol e^-/mol Fe(II) for TCAAP and Tinker AFB columns, respectively; Table 1). This suggests that either (i) reactive Fe(II) was removed from the column, (ii) the transport of dithionite or DNAN to mineral surfaces was restricted by conditions within the column, or (iii) the extent of mineral reduction was affected by the rate of dithionite decomposition.

Flow-through systems introduce the potential for newly generated Fe(II) or other reducible species to be removed from the column before association with mineral surfaces or pollutant reduction occurs. Monitoring aqueous Fe(II) in column effluents, however, negligible losses of Fe(II) from the column were observed during and after exposure to dithionite (Figure S4). Only 1.6 and 5.3 μmol Fe(II) in TCAAP columns and 2.6 and 4.0 μmol Fe(II) in Tinker AFB columns were removed during the first and fifth exposures to dithionite, respectively, corresponding to 0.06–0.20% (w/w) of Fe_T. This suggests that Fe(II) generated during ISCR was mostly retained within the column either because it was not released from the mineral surfaces or it was effectively adsorbed by or bound within the materials within the column. The presence of silicates may also indicate a portion of Fe(II) that is not readily removed from natural soils and sediments. The consistency of breakthrough curves during the five cycles of ISCR and DNAN exposure (Figures S3) indicates that the removal of reduction equivalents by column flow likely did not affect the potential for contaminant reduction.

It is also possible that the transport of reducing equivalents or pollutants to mineral surfaces is restricted in confined systems composed of heterogenous media.[91] Moreover, the iron content of natural sediments can be distributed throughout the bulk mineral as opposed to being concentrated

at singly-coordinated oxygen atoms on mineral surfaces, leaving Fe(III) inaccessible to dithionite. To account for these potential limitations, the columns in this study were packed to a uniform porosity (0.44 ± 0.05), bulk density (1.66 ± 0.04 g cm^{-3}), and particle density (2.68 ± 0.05 g cm^{-3}) to resemble typical subsurface conditions in sandy soils similar to the TCAAP and Tinker AFB (Table S2).[69] The dispersion coefficients in TCAAP (2.37 ± 0.22 cm^2 s^{-1}) and Tinker AFB (2.53 ± 12 cm^{-2} s^{-1}) columns were also determined and indicated advection-dominated regimes with negligible effects from flow retardation.[92] Column porosities and dispersion coefficients were remeasured following all experiments and were not appreciably different from the initial values (Table S2), indicating that ISCR did not affect the physical properties of columns or restrict material transport.

Lastly, the decomposition of dithionite can unevenly distribute iron reduction by ISCR in columns. In batch reactors, the entire supply of dithionite was simultaneously exposed to all of the solid material in a well-mixed heterogenous suspension, whereas, in columns only the materials located immediately following the inlet were exposed to unreacted dithionite. Because dithionite undergoes rapid disproportionation in aqueous media, the combination of Fe(III) reduction and dithionite decomposition limits mineral reduction at locations away from the point of application.[11,48] These differences explain the difference between the batch and column experiments and provide an explanation for the lower extent of DNAN reduction in the column.

^{15}N fractionation during DNAN reduction. DNAN reduction in batch reactors introduced strong ^{15}N enrichment in the remaining contaminant with variations in magnitude comparable to those observed in earlier studies (Figure 3). ^{15}N isotope enrichment factors, ε_N, ranged from -11.1 ± 4.3‰ to -21.5 ± 2.6‰ corresponding to ^{15}N-AKIEs of 1.023 ± 0.009 to 1.045 ± 0.005 (eq. 3).

Because no bonds to C atoms are involved during the reactions leading to nitro-group reduction, C isotope fractionation was small and resulted in secondary ^{13}C-AKIE values (1.0005 ± 0.0002). These results are typical for nitro-group reduction on NACs by Fe(II) species associated with minerals (i.e., large ^{15}N-AKIE = 1.030–1.045 and ^{13}C-AKIE close to unity).[43–45,74] The variability of isotope effects is related to uncertainties associated with experimental and data evaluation procedures such as a different number of samples with variable extent of reactant conversion included in the regression analysis.[59] We postulate these effects as the likely sources of variation in ε_N values reported for experiments with reduced sediments (Figure 3). In fact, our previous report of DNAN reduction by iron (oxyhydr)oxides revealed ε_N values between -9 ± 2‰ and -19 ± 1‰ corresponding to ^{15}N-AKIEs of 1.018 ± 0.002 and 1.039 ± 0.001, respectively, as well as the small ε_C and ^{13}C-AKIE values that are consistent with previous studies.[40] The kinetics of electron and proton transfers preceding the isotope sensitive step of aromatic nitro-group reduction could also lead to variation of ^{15}N-AKIE through partially masking of the isotopically sensitive bond cleavage reaction(s)[45,74,93] and smaller ^{15}N-AKIEs were found with increasing rates of NAC reduction.[45] However, no such trends were observed in our studies with DNAN (Table S3) and further investigation of this phenomenon is beyond the scope of this work.

The agreement in combined ^{15}N- and ^{13}C-AKIEs between this and other reports of abiotic NAC reduction[43–45] suggests that DNAN reduction followed the same reaction mechanism (i.e., nitro-group reduction) in the presence of Fe(II)-amended synthetic and natural materials and with the naturally collected materials after ISCR. Dual-element isotope analysis (δ^{15}N vs δ^{13}C) was used to support this interpretation by illustrating the distinction of our results from other known DNAN transformation pathways (Figure S5).[57] For example, the correlation slope ($\Lambda^{N/C}$) calculated from this study was 43.8 ± 28.6 (38.9 ± 4.3 calculated based on Ojeda et al.[62]) which is in clear contrast

406 with independent evidence from biodegradation ($\Lambda^{N/C} = 0.87 \pm 0.15$) and alkaline hydrolysis ($\Lambda^{N/C}$
407 $= 0.46 \pm 0.04$) experiments.[57] We previously reported a similar $\Lambda^{N/C}$ of 50.5 ± 23.2 during Fe(II)-
408 mediated DNAN reduction by synthetic iron (oxyhydr)oxides.[40]

409

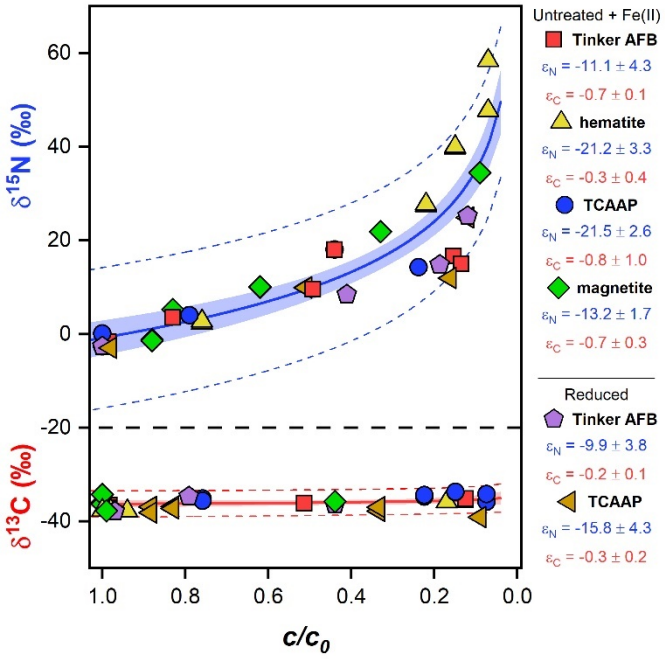

410

411 **Figure 3.** Nitrogen ($\delta^{15}N$) and carbon ($\delta^{13}C$) isotope signatures vs fraction of remaining substrate
412 (c/c_0) during DNAN reduction by iron-bearing minerals. Solid lines represent fits from nonlinear
413 regression with shaded portions indicating the 95% confidence intervals. Dashed lines designate
414 95% prediction intervals. N and C isotope enrichment factors (ε_N, ε_C) were determined from non-
415 linear regression of the data points for each mineral type. Data are shown for untreated materials
416 in the presence of Fe(II) and dithionite-treated materials.

417

418 **Quantifying DNAN transformation from ^{15}N enrichment in the residual contaminant.** As
419 shown in Figures 2a-b, $\delta^{15}N$ values of DNAN at the breakthrough front (~5 pore volumes) were
420 isotopically enriched in ^{15}N corresponding to an increase of $\delta^{15}N$ by 15–20‰. Measured values
421 subsequently decreased and approached the value for unreacted DNAN (-2.4 ± 0.1‰) as the
422 effluent concentrations approached the input level. This trend of $\delta^{15}N$ is consistent with the elution
423 of an increasing share of DNAN that has not been reduced by surface-associated Fe(II). While the

424 data provide evidence that ISCR promoted DNAN reduction, it should be noted that $\delta^{15}N$ values
425 were not fully restored to the input $\delta^{15}N$ value (–1.9 ± 0.1‰ and -2.2 ± 0.1‰ in columns with
426 TCAAP and Tinker AFB sediment, respectively) suggesting the retention and slow release of
427 enough residual ^{15}N-enriched DNAN from the mineral surfaces to influence the $\delta^{15}N$ after the
428 reaction capacity was exhausted or residual, low level transformation activity.[94–96]

429 Based on the above reasoning for the variability of N isotope fractionation associated with NAC
430 reduction, we aggregated all of our current data[40] for isotope fractionation during Fe(II)-catalyzed
431 DNAN reduction in batch experiments. The combined N isotope ratio measurements resulted in
432 an averaged ε_N^* value of -14.9 ± 1.3‰, which is based on one of the most comprehensive data sets
433 for the stable N isotope fractionation related to the transformation of a single nitroaromatic
434 contaminant (Figure S6a). This value was used to establish a quantitative relationship of c/c_0 vs
435 $\Delta^{15}N$ (Figure S6b) to estimate the amount of DNAN degradation from $\delta^{15}N$ measurements made
436 during column experiments (Figure 2a-b). Values of ε_N calculated from TCAAP (-8.6 ± 1.8‰) and
437 Tinker AFB (-7.2 ± 0.8‰) column experiments were lower than batch experiments which could
438 indicate longitudinal mixing with unreacted DNAN in the feed solution. This interpretation agrees
439 with systematic evaluations of the applicability of eq. 2 to assess contaminant transformation in
440 groundwater plumes,[97] where physical heterogeneity, geometry of the contaminant plume, and the
441 extent of degradation can lead to an underestimation of isotope enrichment factors.

442 Application of the higher average ε_N^* value of -14.9 ± 1.3‰ from batch experiments for the
443 evaluation of the extent of DNAN reduction in the sediment columns from the $\Delta^{15}N$ of DNAN
444 leads to predicted values that differ from the actual extent of conversion (Figure 4). A linear
445 regression of predicted versus measured quantities showed a correlation slope of 1.27 ± 0.18 (r^2 =
446 0.96). By not forcing the regression through zero, predicted values overestimate the extent of

conversion at high c/c_0 and underestimate conversion at low c/c_0. While the mean absolute error (MAE) is 0.091 ± 0.063 in c/c_0, the inset in Figure 4 reveals that the relative error is greater at larger conversions and illustrates that in our laboratory model system, the accuracy of the assessment of the extent of degradation decreases with increasing turnover of the contaminant. That said, underprediction of the extent of conversion at low c/c_0 provides a margin of safety.

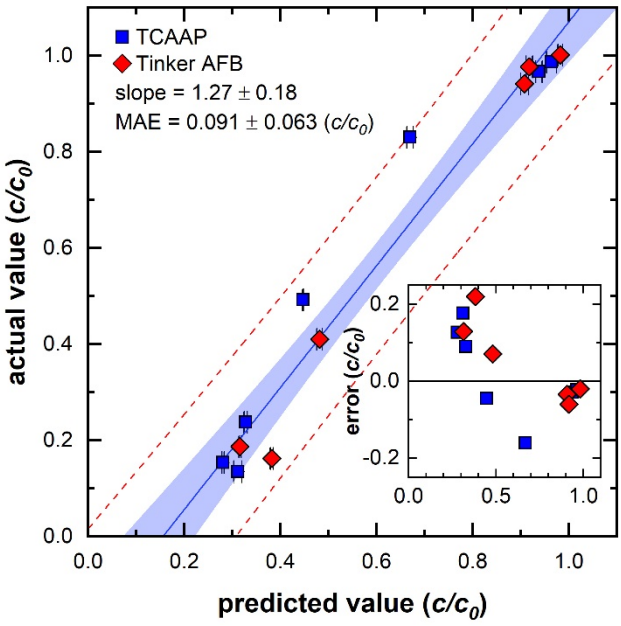

Figure 4. Predicted versus measured values of DNAN transformation by chemically reduced TCAAP and Tinker AFB materials in column reactors. Predictions were made according to eq 2 using an ε_N^* value of -14.9‰. The solid line indicates the calculated fit by linear regression. Shaded portions indicate 95% confidence intervals of linear regressions and dashed lines represent the 95% prediction intervals. The inset shows the prediction error of each estimate.

While a number of additional factors pertinent to the hydrology of the contaminated subsurface will contribute to the successful application of CSIA,[98] Figure 4 illustrates that under the assumption that the same reaction is occurring, there is a basis for using the N isotope fractionation of DNAN measured during laboratory experiments as a proxy of transformation in the field. To confirm the specificity of our model to N isotope fractionation associated with DNAN reduction,

465 we also measured the accompanying $\delta^{13}C$ values of DNAN to the $\delta^{15}N$ data shown in Figure 2a-
466 b. The observed minimal C isotope fractionation of DNAN at the breakthrough front ($\Delta^{13}C < \sim 3‰$;
467 data in Figure S7) is in agreement with the postulated reduction reaction. Because this C isotope
468 fractionation was not observable after 6-7 pore volumes where N isotope fractionation continued,
469 we also consider it unlikely that another reaction such as concurrent (bio)degradation processes
470 contributed to our observations where C isotope fractionation would be more substantial based on
471 the reported ε_C of –3‰ vs. –0.3‰ shown in Figure 3.[57] The distribution of $\delta^{13}C$ against $\delta^{15}N$ from
472 column experiments also reflected the batch systems (Figures 3 and S5) and supports that, in both
473 cases, abiotic reduction was the primary reactive pathway. While we cannot exclude small
474 contributions of sorption processes to the observed DNAN isotope fractionation in dithionite
475 treated columns, data with untreated sediment (Figure S2) suggest that this process is of minor
476 importance.
477
478 **Environmental significance.** Our study investigated laboratory conditions and future work
479 should address direct applications of CSIA to contaminated field sites receiving ISCR. In addition,
480 to assess the efficiency of sediment reduction with external electron donors such as dithionite,
481 these analyses will have to include critical phenomena which we were not able to evaluate in a
482 laboratory model system. Several studies have shown that mass transport related processes
483 including diffusive isotope fractionation, hydrodynamic dispersion, multiple contaminant sources,
484 and the quality of stable isotope ratio measurements can lead to both over- and underestimations
485 of the extent of contaminant degradation.[98–101] For ISCR, the understanding of the local
486 hydrogeology will be necessary to accurately estimate the extent of contaminant (bio)degradation
487 with CSIA.

As remediation strategies are implemented, the adaptation of CSIA for pollutant monitoring in treated soil, sediment, and groundwater is critical for its successful integration into protocols for monitored natural attenuation and active remediation. To an extent, this has been accomplished for the assessment of biodegradation of nitroaromatic explosives in soil.[28] In this work, we reported CSIA as a robust technique to quantify abiotic DNAN reduction in systems receiving repeated dithionite treatments, but future work should include a survey of other *in situ* abiotic remediation strategies (e.g., calcium polysulfides,[13] sodium persulfate[102]). The observation that isotope fractionation is unaffected by natural subsurface materials and ISCR can be leveraged to generate accurate estimates of contaminant removal strengthen our findings. Moreover, it provides strong support for the compulsory lines of evidence set by the US Environmental Protection Agency for evaluating the progress of natural attenuation.[27] Considering DNAN as a surrogate for other NACs allows for this approach to be applied to a wide range of environmental pollutants.

ACKNOWLEDGEMENTS

This work was supported by the Strategic Environmental Research and Development Program (SERDP, Project No. ER2618). Thanks to Lee Penn (UMN, Department of Chemistry) for allowing use of the X-ray diffractometer and to Jeanette L. Voelz (UMN, Department of Chemistry) for providing the hematite nanoparticles used in this study. ICP-OES analyses were performed by Clare Johnston (UMN, Department of Chemistry).

ASSOCIATED CONTENT

Supporting Information

A detailed report of additional analytical methods, materials synthesis and characterization techniques, batch reaction procedures, CSIA calculations, and further kinetics and isotope results. The files are available free of charge via the internet at https://pubs.acs.org/journal/esthag.

The authors declare no competing interests.

REFERENCES

(1) Ferrey, M. L.; Wilkin, R. T.; Ford, R. G.; Wilson, J. T. Nonbiological Removal of Cis-Dichloroethylene and 1,1-Dichloroethylene in Aquifer Sediment Containing Magnetite. *Environ. Sci. Technol.* **2004**, *38* (6), 1746–1752.

(2) Hofstetter, T. B.; Heijman, C. G.; Haderlein, S. B.; Holliger, C.; Schwarzenbach, R. P. Complete Reduction of TNT and Other (Poly)Nitroaromatic Compounds under Iron-Reducing Subsurface Conditions. *Environ. Sci. Technol.* **1999**, *33* (9), 1479–1487.

(3) Hofstetter, T. B.; Neumann, A.; Schwarzenbach, R. P. Reduction of Nitroaromatic Compounds by Fe (II) Species Associated with Iron-Rich Smectites. *Environ. Sci. Technol.* **2006**, *40* (1), 235–242.

(4) Hofstetter, T. B.; Schwarzenbach, R. P.; Haderlein, S. B. Reactivity of Fe(II) Species Associated with Clay Minerals. *Environ. Sci. Technol.* **2003**, *37* (3), 519–528.

(5) Butler, E. C.; Hayes, K. F. Effects of Solution Composition and PH on the Reductive Dechlorination of Hexachloroethane by Iron Sulfide. *Environ. Sci. Technol.* **1998**, *32*,

1276–1284.

(6) Schaefer, C. E.; Ho, P.; Berns, E.; Werth, C. Mechanisms for Abiotic Dechlorination of Trichloroethene by Ferrous Minerals under Oxic and Anoxic Conditions in Natural Sediments. *Environ. Sci. Technol.* **2018**, *52* (23), 13747–13755.

(7) Simpanen, S.; Dahl, M.; Gerlach, M.; Mikkonen, A.; Malk, V.; Mikola, J.; Romantschuk, M. Biostimulation Proved to Be the Most Efficient Method in the Comparison of in Situ Soil Remediation Treatments after a Simulated Oil Spill Accident. *Environ. Sci. Pollut. Res.* **2016**, *23* (24), 25024–25038.

(8) McGuire, T. M.; Adamson, D. T.; Burcham, M. S.; Bedient, P. B.; Newell, C. J. Evaluation of Long-Term Performance and Sustained Treatment at Enhanced Anaerobic Bioremediation Sites. *Groundw. Monit. Remediat.* **2016**, *36* (2), 32–44.

(9) Wu, Y.-J.; Liu, P.-W. G.; Hsu, Y.-S.; Whang, L.-M.; Lin, T.-F.; Hung, W.-N.; Cho, K.-C. Application of Molecular Biological Tools for Monitoring Efficiency of Trichloroethylene Remediation. *Chemosphere* **2019**, *233*, 697–704.

(10) Schaefer, C. E.; Lavorgna, G. M.; Haluska, A. A.; Annable, M. D. Long-Term Impacts on Groundwater and Reductive Dechlorination Following Bioremediation in a Highly Characterized Trichloroethene DNAPL Source Area. *Groundw. Monit. Remediat.* **2018**, *38* (3), 65–74.

(11) Amonette, J. E.; Szecsody, J. E.; Schaef, H. T.; Templeton, J. C.; Gorby, Y. A.; Fruchter, J. S. *Abiotic Reduction of Aquifer Materials by Dithionite: A Promising in-Situ Remediation Technology*; Richland, WA, USA, 1994.

551 (12) Fruchter, J. S. J. S.; Cole, C. R. C. R.; Williams, M. D. M. D.; Vermeul, V. R.; Amonette,
552 J. E. J. E.; Szecsody, J. E.; Istok, J. D.; Humphrey, M. D. Creation of a Subsurface
553 Permeable Treatment Zone for Aqueous Chromate Contamination Using In Situ Redox
554 Manipulation. *Groundw. Monit. Remediat.* **2000**, *20* (2), 66–77.

555 (13) Graham, M. C.; Farmer, J. G.; Anderson, P.; Paterson, E.; Hillier, S.; Lumsdon, D. G.;
556 Bewley, R. J. F. Calcium Polysulfide Remediation of Hexavalent Chromium Contamination
557 from Chromite Ore Processing Residue. *Sci. Total Environ.* **2006**, *364* (1–3), 32–44.

558 (14) Fan, D.; O'Brien Johnson, G.; G. Tratnyek, P.; L. Johnson, R. Sulfidation of Nano
559 Zerovalent Iron (NZVI) for Improved Selectivity During In-Situ Chemical Reduction
560 (ISCR). *Environ. Sci. Technol.* **2016**, *50* (17), 9558–9565.

561 (15) Han, Y.; Yan, W. Reductive Dechlorination of Trichloroethene by Zero-Valent Iron
562 Nanoparticles: Reactivity Enhancement through Sulfidation Treatment. *Environ. Sci.*
563 *Technol.* **2016**, *50* (23), 12992–13001.

564 (16) Niedźwiecka, J. B.; Finneran, K. T. Combined Biological and Abiotic Reactions with Iron
565 and Fe(III)-Reducing Microorganisms for Remediation of Explosives and Insensitive
566 Munitions (IM). *Environ. Sci. Water Res. Technol* **2015**, *1*, 34–39.

567 (17) D. Ludwig, R.; Su, C.; R. Lee, T.; T. Wilkin, R.; D. Acree, S.; R. Ross, R.; Keeley, A. In
568 Situ Chemical Reduction of Cr(VI) in Groundwater Using a Combination of Ferrous Sulfate
569 and Sodium Dithionite: A Field Investigation. *Environ. Sci. Technol.* **2007**, *41* (15), 5299–
570 5305.

571 (18) Dresel, P. E.; Wellman, D. M.; Cantrell, K. J.; Truex, M. T. Review: Technical and Policy

572 Challenges in Deep Vadose Zone Remediation of Metals and Radionuclides. *Environ. Sci.*
573 *Technol.* **2011**, *45* (10), 4207–4216.

574 (19) Szecsody, J. E.; Fruchter, J. S.; Williams, M. D.; Vermeul, V. R.; Sklarew, D. In Situ
575 Chemical Reduction of Aquifer Sediments: Enhancement of Reactive Iron Phases and TCE
576 Dechlorination. *Environ. Sci. Technol.* **2004**, *38* (17), 4656–4663.

577 (20) Brown, R. A.; Mueller, J. G.; Seech, A.G.; Henderson, J. K.; Wilson, J. T. Interactions
578 between biological and abiotic pathways in the reduction of chlorinated solvents.
579 *Remediation*, **2009**, *20* (1), 9-20.

580 (21) McKelvie, J. R.; Mackay, D. M.; de Sieyes, N. R.; Lacrampe-Couloume, G.; Sherwood
581 Lollar, B. Quantifying MTBE Biodegradation in the Vandenberg Air Force Base Ethanol
582 Release Study Using Stable Carbon Isotopes. *J. Contam. Hydrol.* **2007**, *94* (3–4), 157–165.

583 (22) Chartrand, M.; Passeport, E.; Rose, C.; Lacrampe-Couloume, G.; Bidleman, T. F.; Jantunen,
584 L. M.; Sherwood Lollar, B. Compound Specific Isotope Analysis of
585 Hexachlorocyclohexane Isomers: A Method for Source Fingerprinting and Field
586 Investigation of in Situ Biodegradation. *Rapid Commun. Mass Spectrom.* **2015**, *29* (6), 505–
587 514.

588 (23) Bosma, T. N. P.; Middeldorp, P. J. M.; Schraa, G.; Zehnder, A. J. B. Mass Transfer
589 Limitation of Biotransformation: Quantifying Bioavailability. *Environ. Sci. Technol.* **1997**,
590 *31* (1), 248–252.

591 (24) Torrent, J.; Schwertmann, U.; Barron, V. The Reductive Dissolution of Synthetic Goethite
592 and Hematite in Dithionite. *Clay Miner.* **1987**, *22* (3), 329–337.

593 (25) Yang, L.; I. Steefel, C.; A. Marcus, M.; R. Bargar, J. Kinetics of Fe(II)-Catalyzed
594 Transformation of 6-Line Ferrihydrite under Anaerobic Flow Conditions. *Environ. Sci.*
595 *Technol.* **2010**, *44* (14), 5469–5475.

596 (26) Amstaetter, K.; Borch, T.; Larese-Casanova, P.; Kappler, A. Redox Transformation of
597 Arsenic by Fe(II)-Activated Goethite (α-FeOOH). *Environ. Sci. Technol.* **2009**, *44* (1), 102–
598 108.

599 (27) Hunkeler, D.; Meckenstock, R. U.; Lollar, B. S.; Schmidt, T. C.; Wilson, J. T. *A Guide for*
600 *Assessing Biodegradation and Source Identification of Organic Ground Water*
601 *Contaminants Using Compound Specific Isotope Analysis (CSIA)*; Oklahoma, USA, 2008.

602 (28) Wijker, R. S.; Bolotin, J.; Nishino, S. F.; Spain, J. C.; Hofstetter, T. B. Using Compound-
603 Specific Isotope Analysis to Assess Biodegradation of Nitroaromatic Explosives in the
604 Subsurface. *Environ. Sci. Technol.* **2013**, *47* (13), 6872–6883.

605 (29) Meckenstock, R. U.; Morasch, B.; Griebler, C.; Richnow, H. H. Stable Isotope Fractionation
606 Analysis as a Tool to Monitor Biodegradation in Contaminated Acquifers. *J. Contam.*
607 *Hydrol.* **2004**, *75* (3–4), 215–255.

608 (30) Sherwood Lollar, B.; Slater, G. F.; Sleep, B.; Witt, M.; Klecka, G. M.; Harkness, M.;
609 Spivack, J. Stable Carbon Isotope Evidence for Intrinsic Bioremediation of
610 Tetrachloroethene and Trichloroethene at Area 6, Dover Air Force Base. *Environ. Sci.*
611 *Technol.* **2000**, *35* (2), 261–269.

612 (31) Thullner, M.; Richnow, H. H.; Fischer, A. Characterization and Quantification of in Situ
613 Biodegradation of Groundwater Contaminants Using Stable Isotope Fractionation Analysis:

614 Advantages and Limitations. In *Environmental and Regional Air Pollution*; Nova Science
615 Publishers, 2009.

616 (32) Alvarez-Zaldívar, P.; Centler, F.; Maier, U.; Thullner, M.; Imfeld, G. Biogeochemical
617 Modelling of in Situ Biodegradation and Stable Isotope Fractionation of Intermediate
618 Chloroethenes in a Horizontal Subsurface Flow Wetland. *Ecol. Eng.* **2016**, *90*, 170–179.

619 (33) Elsner, M.; Zwank, L.; Hunkeler, D.; Schwarzenbach, R. P. A New Concept Linking
620 Observable Stable Isotope Fractionation to Transformation Pathways of Organic Pollutants.
621 *Environ. Sci. Technol.* **2005**, *39* (18), 6896–6916.

622 (34) Schmidt, T. C.; Zwank, L.; Elsner, M.; Berg, M.; Meckenstock, R. U.; Haderlein, S. B.
623 Compound-Specific Stable Isotope Analysis of Organic Contaminants in Natural
624 Environments: A Critical Review of the State of the Art, Prospects, and Future Challenges.
625 *Anal. Bioanal. Chem.* **2004**, *378* (2), 283–300.

626 (35) Wijker, R. S.; Zeyer, J.; Hofstetter, T. B. Isotope Fractionation Associated with the
627 Simultaneous Biodegradation of Multiple Nitrophenol Isomers by Pseudomonas Putida B2.
628 *Environ. Sci. Process. Impacts* **2017**, *19* (5), 775–784.

629 (36) Sherwood Lollar, B.; Slater, G.; Ahad, J.; Sleep, B.; Spivack, J.; Brennan, M.; MacKenzie,
630 P. Contrasting Carbon Isotope Fractionation during Biodegradation or Trichloroethylene
631 and Toluene: Implications for Intrinsic Bioremediation. *Org. Geochem.* **1999**, *30*, 813–820.

632 (37) Aeppli, C.; B. Hofstetter, T.; I. F. Amaral, H.; Kipfer, R.; P. Schwarzenbach, R.; Berg, M.
633 Quantifying In Situ Transformation Rates of Chlorinated Ethenes by Combining
634 Compound-Specific Stable Isotope Analysis, Groundwater Dating, And Carbon Isotope

635 Mass Balances. *Environ. Sci. Technol.* **2010**, *44* (10), 3705–3711.

636 (38) Dodard, S. G.; Sarrazin, M.; Hawari, J.; Paquet, L.; Ampleman, G.; Thiboutot, S.; Sunahara,
637 G. I. Ecotoxicological Assessment of a High Energetic and Insensitive Munitions
638 Compound: 2,4-Dinitroanisole (DNAN). *J. Hazard. Mater.* **2013**, *262*, 143–150.

639 (39) Johnson, M. S.; Eck, W. S.; Lent, E. M. Toxicity of Insensitive Munition (IMX)
640 Formulations and Components. *Propellants, Explos. Pyrotech.* **2017**, *42* (1), 9–16.

641 (40) Berens, M. J.; Ulrich, B. A.; Strehlau, J. H.; Hofstetter, T. B.; Arnold, W. A. Mineral
642 Identity, Natural Organic Matter, and Repeated Contaminant Exposures Do Not Affect the
643 Carbon and Nitrogen Isotope Fractionation of 2,4-Dinitroanisole during Abiotic Reduction.
644 *Environ. Sci. Process. Impacts* **2019**, *21*, 51–62.

645 (41) Boparai, H. K.; Comfort, S. D.; Shea, P. J.; Szecsody, J. E. Remediating Explosive-
646 Contaminated Groundwater by in Situ Redox Manipulation (ISRM) of Aquifer Sediments.
647 *Chemosphere* **2008**, *71* (5), 933–941.

648 (42) He, F.; Zhao, D.; Paul, C. Field Assessment of Carboxymethyl Cellulose Stabilized Iron
649 Nanoparticles for in Situ Destruction of Chlorinated Solvents in Source Zones. *Water Res.*
650 **2010**, *44* (7), 2360–2370.

651 (43) Hofstetter, T. B.; Neumann, A.; Arnold, W. A.; Hartenbach, A. E.; Bolotin, J.; Cramer, C.
652 J.; Schwarzenbach, R. P. Substituent Effects on Nitrogen Isotope Fractionation during
653 Abiotic Reduction of Nitroaromatic Compounds. *Environ. Sci. Technol.* **2008**, *42* (6), 1997–
654 2003.

655 (44) Hartenbach, A.; Hofstetter, T. B.; Berg, M.; Bolotin, J.; Schwarzenbach, R. P. Using

Nitrogen Isotope Fractionation to Assess Abiotic Reduction of Nitroaromatic Compounds. *Environ. Sci. Technol.* **2006**, *40* (24), 7710–7716.

(45) Hartenbach, A. E.; Hofstetter, T. B.; Aeschbacher, M.; Sander, M.; Kim, D.; Strathmann, T. J.; Arnold, W. A.; Cramer, C. J.; Schwarzenbach, R. P. Variability of Nitrogen Isotope Fractionation during the Reduction of Nitroaromatic Compounds with Dissolved Reductants. *Environ. Sci. Technol.* **2008**, *42* (22), 8352–8359.

(46) Pichtel, J. Distribution and Fate of Military Explosives and Propellants in Soil: A Review. *Appl. Environ. Soil Sci.* **2012**, *2012* (2012).

(47) Albright, R. D. *Cleanup of Chemical and Explosive Munitions - Locating, Identifying Contaminants, and Planning for Environmental Remediation of Land and Sea Military Ranges and Ordnance Dumpsites*, 2nd ed.; William Andrew: Norwich, NY, USA, 2012.

(48) Istok, J. D.; Amonette, J. E.; Cole, C. R.; Fruchter, J. S.; Humphrey, M. D.; Szecsody, J. E.; Teel, S. S.; Vermeul, V. R.; Williams, M. D.; Yabusaki, S. B. In Situ Redox Manipulation by Dithionite Injection: Intermediate-Scale Laboratory Experiments. *Ground Water* **1999**, *37*, 884–889.

(49) Hocking, G.; Givens, M. A.; Thurman, C. M.; Lacko, C. M. Installation of Permeable Reactive Barrier at Tinker Air Force Base, Oklahoma City, Oklahoma. In *5th International Conference on Remediation of Chlorinated and Recalcitrant Compounds*; Monterey, CA, 2006.

(50) Voelz, J.; Arnold, W. A.; Penn, R. L. Redox-Induced Nucleation and Growth of Goethite on Synthetic Hematite Nanoparticles. *Am. Mineral.* **2018**, *103*, 1021–1029.

677 (51) Strehlau, J. H.; Berens, M. J.; Arnold, W. A. Mineralogy and Buffer Identity Effects on
678 RDX Kinetics and Intermediates during Reaction with Natural and Synthetic Magnetite.
679 *Chemosphere* **2018**, *213*, 602–609.

680 (52) Cornell, R. M.; Giovanoli, R. Acid Dissolution of Hematites of Different Morphologies.
681 *Clay Miner.* **1993**, *28* (2), 223–232.

682 (53) Cornell, R. M.; Giovanoli, R. Acid Dissolution of Akaganeite and Lepidocrocite: The Effect
683 on Crystal Morphology. *Clays Clay Miner.* **1988**, *36* (5), 385–390.

684 (54) Viollier, E.; Inglett, P. W.; Hunter, K.; Roychoudhury, A. N.; Van Cappellen, P. The
685 Ferrozine Method Revisited: Fe(II)/Fe(III) Determination in Natural Waters. *Appl.*
686 *Geochemistry* **2000**, *15* (6), 785–790.

687 (55) Sumner, M. E.; Miller, W. P. Cation Exchange Capacity and Exchange Coefficients. In
688 *Methods of Soil Analysis Part 3 - Chemical Methods*; 1996; pp 1201–1229.

689 (56) Berg, M.; Bolotin, J.; Hofstetter, T. B. Compound-Specific Nitrogen and Carbon Isotope
690 Analysis of Nitroaromatic Compounds in Aqueous Samples Using Solid-Phase
691 Microextraction Coupled to GC/IRMS. *Anal. Chem.* **2007**, *79* (6), 2386–2393.

692 (57) Ulrich, B. A.; Palatucci, M.; Bolotin, J.; Spain, J. C.; Hofstetter, T. B. Different Mechanisms
693 of Alkaline and Enzymatic Hydrolysis of the Insensitive Munition Component 2,4-
694 Dinitroanisole Lead to Identical Products. *Environ. Sci. Technol. Lett.* **2018**, *5* (7), 456–461.

695 (58) Kremser, A.; Jochmann, M. A.; Schmidt, T. C. PAL SPME Arrow - Evaluation of a Novel
696 Solid-Phase Microextraction Device for Freely Dissolved PAHs in Water. *Anal. Bioanal.*
697 *Chem.* **2016**, *408* (3), 943–952.

(59) Pati, S. G.; Kohler, H.-P. E.; Hofstetter, T. B. Characterization of Substrate, Cosubstrate, and Product Isotope Effects Associated with Enzymatic Oxygenations of Organic Compounds Based on Compound-Specific Isotope Analysis. In *Methods in Enzymology*; Elsevier Inc., 2017; Vol. 596, pp 291–329.

(60) Schimmelmann, A.; Albertino, A.; Sauer, P. E.; Qi, H.; Molinie, R.; Mesnard, F. Nicotine, Acetanilide and Urea Multi-Level 2H-, 13C- and 15N-Abundance Reference Materials for Continuous-Flow Isotope Ratio Mass Spectrometry. *Rapid Commun. Mass Spectrom.* **2009**, *23* (22), 3513–3521.

(61) Elsner, M. Stable Isotope Fractionation to Investigate Natural Transformation Mechanisms of Organic Contaminants: Principles, Prospects and Limitations. *J. Environ. Monit.* **2010**, *12* (11), 2005–2031.

(62) Ojeda, A. S.; Phillips, E.; Mancini, S. A.; Sherwood Lollar, B. Sources of Uncertainty in Biotransformation Mechanistic Interpretations and Remediation Studies Using CSIA. *Anal. Chem.* **2019**, *91* (14), 9147–9153.

(63) G. B. Williams, A.; M. Scherer, M. Spectroscopic Evidence for Fe(II)−Fe(III) Electron Transfer at the Iron Oxide−Water Interface. *Environ. Sci. Technol.* **2004**, *38* (18), 4782–4790.

(64) Klausen, J. J.; Tröber, S. P.; Haderlein, S. B.; Schwarzenbach, R. P.; Troeber, S. P.; Haderlein, S. B.; Schwarzenbach, R. P. Reduction of Substituted Nitrobenzenes by Fe(II) in Aqueous Mineral Suspensions. *Environ. Sci. Technol.* **1995**, *29* (9), 2396–2404.

(65) Amonette, J. E.; Workman, D. J.; Kennedy, D. W.; Fruchter, J. S.; Gorby, Y. A.

719 Dechlorination of Carbon Tetrachloride by Fe(II) Associated with Goethite. *Environ. Sci.*
720 *Technol.* **2000**, *34* (21), 4606–4613.

721 (66) Elsner, M.; Schwarzenbach, R. P.; Haderlein, S. B. Reactivity of Fe(II)-Bearing Minerals
722 toward Reductive Transformation of Organic Contaminants. *Environ. Sci. Technol.* **2004**,
723 *38* (3), 799–807.

724 (67) Fan, D.; J. Bradley, M.; W. Hinkle, A.; L. Johnson, R.; G. Tratnyek, P. Chemical Reactivity
725 Probes for Assessing Abiotic Natural Attenuation by Reducing Iron Minerals. *Environ. Sci.*
726 *Technol.* **2016**, *50* (4), 1868–1876.

727 (68) Voelz, J. L.; Johnson, N. W.; Chun, C. L.; Arnold, W. A.; Penn, R. L. Quantitative
728 Dissolution of Environmentally Accessible Iron Residing in Iron-Rich Minerals: A Review.
729 *ACS Earth Sp. Chem.* **2019**, *3* (8), 1371–1392.

730 (69) Essington, M. E. *Soil and Water Chemistry: An Integrative Approach*, 2nd ed.; CRC Press,
731 2015.

732 (70) Guo, H.; Barnard, A. S. Naturally Occurring Iron Oxide Nanoparticles: Morphology,
733 Surface Chemistry and Environmental Stability. *J. Mater. Chem. A* **2013**, *1* (January 2013),
734 27–42.

735 (71) Schwertmann, U.; Cornell, R. M. *Iron Oxides in the Laboratory: Preparation and*
736 *Characterization*, 2nd ed.; Wiley-VCH: Weinheim, 2000.

737 (72) Strehlau, J. H.; Toner, B. M.; Arnold, W. A.; Penn, R. L. Accessible Reactive Surface Area
738 and Abiotic Redox Reactivity of Iron Oxyhydroxides in Acidic Brines. *Geochim.*
739 *Cosmochim. Acta* **2017**, *197*, 345–355.

740 (73) James, B. R.; Brose, D. A. Oxidation-Reduction Phenomena. In *Handbook of Soil Science:*
741 *Properties and Processes*; CRC Press: Boca Raton, FL, 2012; pp 14-1-14–24.

742 (74) Gorski, C. A.; Nurmi, J. T.; Tratnyek, P. G.; Hofstetter, T. B.; Scherer, M. M. Redox
743 Behavior of Magnetite: Implications for Contaminant Reduction. *Environ. Sci. Technol.*
744 **2010**, *44* (1), 55–60.

745 (75) Gorski, C. A.; Scherer, M. M. Influence of Magnetite Stoichiometry on FeII Uptake and
746 Nitrobenzene Reduction. *Environ. Sci. Technol.* **2009**, *43* (10), 3675–3680.

747 (76) Haggstrom, L.; Annersten, H.; Ericsson, T.; Wappling, R.; Karner, W.; Bjarman, S.
748 Magnetic Dipolar and Electric Quadrupolar Effects on the Mossbauer Spectra of Magnetite
749 above the Verwey Transition. *Hyperfine Interact.* **1977**, *5* (1), 201–214.

750 (77) Vandenberghe, R. E.; Hus, J. J.; De Grave, E. Evidence from Mössbauer Spectroscopy of
751 Neo-Formation of Magnetite/Maghemite in the Soils of Loess/Paleosol Sequences in China.
752 *Hyperfine Interact.* **1998**, *117* (1/4), 359–369.

753 (78) Wehrli, B.; Sulzberger, B.; Stumm, W. Redox Processes Catalyzed by Hydrous Oxide
754 Surfaces. *Chem. Geol.* **1989**, *78* (3–4), 167–179.

755 (79) Torrent, J.; Barron, V. Iron Oxides in Relation to the Colour of Mediterranean Soils. In
756 *Applied Study of Cultural Heritage and Clays*; 2003; pp 377–386.

757 (80) Lovley, D. R.; Coates, J. D.; Blunt-Harris, E. L.; Phillips, E. J. P.; Woodward, J. C. Humic
758 Substances as Electron Acceptors for Microbial Respiration. *Nature* **1996**, *382*, 445–448.

759 (81) Scott, D. T.; Mcknight, D. M.; Blunt-Harris, E. L.; Kolesar, S. E.; Lovley, D. R. Quinone
760 Moieties Act as Electron Acceptors in the Reduction of Humic Substances by Humics-

761 Reducing Microorganisms. *Environ. Sci. Technol.* **1998**, *32* (19), 2984–2989.

762 (82) Lovley, D. R.; Fraga, J. L.; Coates, J. D.; Blunt-Harris, E. L. Humics as an Electron Donor
763 for Anaerobic Respiration. *Environ. Microbiol.* **1999**, *1* (1), 89–98.

764 (83) Ratasuk, N.; A. Nanny, M. Characterization and Quantification of Reversible Redox Sites
765 in Humic Substances. *Environ. Sci. Technol.* **2007**, *41* (22), 7844–7850.

766 (84) M. Dunnivant, F.; P. Schwarzenbach, R.; L. Macalady, D. Reduction of Substituted
767 Nitrobenzenes in Aqueous Solutions Containing Natural Organic Matter. *Environ. Sci.*
768 *Technol.* **1992**, *26* (11), 2133–2141.

769 (85) Deiana, S.; Gessa, C.; Manunza, B.; Rausa, R.; Solinas, V. Iron(III) Reduction by Natural
770 Humic Acids: A Potentiometric and Spectroscopic Study. *Eur. J. Soil Sci.* **1995**, *46* (1),
771 103–108.

772 (86) Beyer, M. E.; Bond, A. M.; McLaughlin, R. J. W. Simultaneous Polarographic
773 Determination of Ferrous, Ferric, and Total Iron in Standard Rocks. *Anal. Chem.* **2002**, *47*
774 (3), 479–482.

775 (87) Haese, R. R.; Wallmann, K.; Dahmke, A.; Kretzmann, U.; Müller, P. J.; Schulz, H. D. Iron
776 Species Determination to Investigate Early Diagenetic Reactivity in Marine Sediments.
777 *Geochim. Cosmochim. Acta* **1997**, *61* (1), 63–72.

778 (88) Neumann, A.; Hofstetter, T. B.; Lüssi, M.; Cirpka, O. A.; Petit, S.; Schwarzenbach, R. P.
779 Assessing the Redox Reactivity of Structural Iron in Smectites Using Nitroaromatic
780 Compounds As Kinetic Probes. *Environ. Sci. Technol.* **2008**, *42* (22), 8381–8387.

781 (89) Erickson, A. J.; Gulliver, J. S.; Arnold, W. A.; Brekke, C.; Bredal, M. Abiotic Capture of

782 Stormwater Nitrates with Granular Activated Carbon. *Environ. Eng. Sci.* **2016**, *33* (5), 354–
783 363.

784 (90) Simon, R.; Colón, D.; L. Tebes-Stevens, C.; J. Weber, E. Effect of Redox Zonation on the
785 Reductive Transformation of P-Cyanonitrobenzene in a Laboratory Sediment Column.
786 *Environ. Sci. Technol.* **2000**, *34* (17), 3617–3622.

787 (91) Freeze, R. A.; Cherry, J. A. *Groundwater*, 1st ed.; Prentice Hall, 1979.

788 (92) Gulliver, J. S. *Introduction to Chemical Transport in the Environment*; Cambridge
789 University Press: Cambridge, 2007.

790 (93) Stewart, S. M.; Hofstetter, T. B.; Joshi, P.; Gorski, C. A. Linking Thermodynamics to
791 Pollutant Reduction Kinetics by Fe2+ Bound Toiron Oxides. *Environ. Sci. Technol.* **2018**,
792 *52* (10), 5600–5609.

793 (94) Haderlein, S. B.; Weissmahr, K. W.; Schwarzenbach, R. P. Specific Adsorption of
794 Nitroaromatic Explosives and Pesticides to Clay Minerals. *Environ. Sci. Technol.* **1996**, *30*
795 (2), 612–622.

796 (95) Arthur, J. D.; Mark, N. W.; Taylor, S.; Šimunek, J.; Brusseau, M. L.; Dontsova, K. M. Batch
797 Soil Adsorption and Column Transport Studies of 2,4-Dinitroanisole (DNAN) in Soils. *J.*
798 *Contam. Hydrol.* **2017**, *199*, 14–23.

799 (96) B. Haderlein, S.; P. Schwarzenbach, R. Adsorption of Substituted Nitrobenzenes and
800 Nitrophenols to Mineral Surfaces. *Environ. Sci. Technol.* **1993**, *27* (2), 316–326.

801 (97) Abe, Y.; Hunkeler, D. Does the Rayleigh Equation Apply to Evaluate Field Isotope Data in
802 Contaminant Hydrogeology? *Environ. Sci. Technol.* **2006**, *40* (5), 1588–1596.

(98) Thullner, M.; Centler, F.; Richnow, H. H.; Fischer, A. Quantification of Organic Pollutant Degradation in Contaminated Aquifers Using Compound Specific Stable Isotope Analysis - Review of Recent Developments. *Org. Geochem.* **2012**, *42* (12), 1440–1460.

(99) Chiogna, G.; Eberhardt, C.; Grathwohl, P.; A. Cirpka, O.; Rolle, M. Evidence of Compound-Dependent Hydrodynamic and Mechanical Transverse Dispersion by Multitracer Laboratory Experiments. *Environ. Sci. Technol.* **2009**, *44* (2), 688–693.

(100) Fischer, A.; Theuerkorn, K.; Stelzer, N.; Gehre, M.; Thullner, M.; H. Richnow, H. Applicability of Stable Isotope Fractionation Analysis for the Characterization of Benzene Biodegradation in a BTEX-Contaminated Aquifer. *Environ. Sci. Technol.* **2007**, *41* (10), 3689–3696.

(101) Thullner, M.; Fischer, A.; Richnow, H. H.; Wick, L. Y. Influence of Mass Transfer on Stable Isotope Fractionation. *Applied Microbiology and Biotechnology*. Springer January 11, 2013, pp 441–452.

(102) Tsitonaki, A.; Petri, B.; Crimi, M.; Mosbk, H.; Siegrist, R. L.; Bjerg, P. L. In Situ Chemical Oxidation of Contaminated Soil and Groundwater Using Persulfate: A Review. *Crit. Rev. Environ. Sci. Technol.* **2010**, *40* (1), 55–91.

821 **TOC Art**

822